On the static and dynamic response of electrostatic actuators

D. ELATA*

Faculty of Mechanical Engineering, Technion – Israel Institute of Technology, Haifa 32000, Israel

Abstract. A systematic approach for analyzing the static and dynamic electromechanical response of electrostatic actuators is presented. The analysis is based on energy methods. An analysis approach for extracting dynamic response parameters of electrostatic actuators, while only considering static states of the system, is presented. This is an efficient method for extracting the dynamic pull-in parameters because it does not require time integration of momentum equations.

Key words: electrostatic actuators, pull-in instability.

1. Introduction

Electrostatic actuators are prevalent in Micro-Electro-Mechanical Systems (MEMS) because they are compatible with microfabrication technology, have a low power consumption, and because electrostatic forces are sufficiently large to drive micro-motors. Electrostatic actuators can be produced using the same micromachining technology that was developed for producing microelectronics systems [1,2] (with the addition of a few new technologies developed primarily for MEMS). Many other types of actuators used in microsystems either require special materials and non-standard fabrication processes (e.g. piezoelectric actuators) or have a large power consumption (e.g. thermoelastic actuators) [3]. In many common products with macroscopic size (i.e. with characteristic size above 1 mm) electromagnetic forces together with axes and sliders are used to construct motors. Axes and sliders are often impractical in microsystems due to issues of reliability and wear. In many microsystems relative motion between different parts of the system is enabled by use of elastic flexures. Flexures are designed to have a high rigidity in all directions in which motion is to be restricted, and a lower rigidity in the directions in which motion is desired. In microsystems, the distance between electrodes that are subjected to different electric potentials is sufficiently small to enable large electrostatic forces. These electrostatic forces are sufficiently large to induce motion of the flexures and therefore enable the construction of micro-motors.

Due to the nonlinear nature of electrostatic forces, the electromechanical response of many electrostatic actuators is nonlinear and their stable range may be limited by the well known pull-in instability [4,5]. The pull-in instability is an unwanted effect when a large stable travel range is required (e.g. [6,7]), but may be a beneficial effect when rapid transition between two states of the system is required (e.g. RF-MEMS switches [8,9]).

Electrostatic switches are currently being developed for RF-MEMS applications, where they have strong advantages over similar components implemented in electronics [8–11].

Much effort has been invested in recent years to develop efficient modelling tools that would facilitate the design process of electrostatic switches and would provide insight on the pull-in instability (e.g. [12–17]).

The parameters of the pull-in state of electrostatic switches are of specific interest in the design process. Time integration of the equation of motion of electrostatic actuators requires much computation time primarily due to nonlinear effects such as electrostatic forces, damping, and more.

Recently, an alternative approach for extracting the pull-in state of electrostatic actuators was proposed [18,19]. This approach is limited to systems with negligible damping but it enables to extract the pull-in parameters of the dynamic response by considering only static states of the system.

The present work reviews energy methods for extracting the static and dynamic pull-in parameters of electrostatic switches. The analysis method is demonstrated by considering the electromechanical response of two model problems of electrostatic actuators with a single degree of freedom, and a third model problem with a more general geometry.

2. Static response of electrostatic actuators

2.1. Static response of the parallel-plates actuator. In this section the static response of an electrostatic actuator with a single degree-of-freedom (DOF) is analyzed. As a simple model problem, consider the parallel-plate actuator illustrated in Fig. 1. The actuator is constructed from a top electrode of mass m and area A that is suspended on a linear elastic spring with stiffness k, above a fixed bottom electrode. The bottom electrode is coated with a dielectric layer of thickness d_0, and the initial gap between the top electrode and the dielectric is g. The two electrodes constitute a deformable capacitor. The fixed bottom electrode is electrically grounded and a voltage V or a charge Q may be applied to the top electrode (charge actuation has been implemented and used to extend the travel range of electrostatic actuators [20,21]).
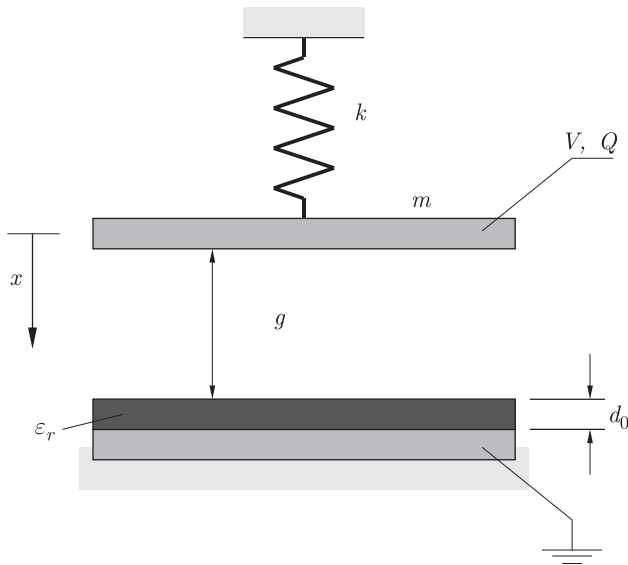
---
*e-mail: elata@tx.technion.ac.il

Fig. 1. Schematic view of the parallel-plates actuator with a dielectric layer coating the bottom electrode

The electromechanical response of the parallel-plates actuator when it is driven by charge Q is determined by the potential of the system

$$\psi_Q(x, Q) = \frac{1}{2}kx^2 + \frac{1}{2}\frac{Q^2}{C(x)} \qquad (1)$$

where x is the DOF of the movable top electrode and $C(x)$ is the capacitance of the system. The two terms on the right hand side of (1) are the mechanical potential of the suspending spring and the electrostatic potential of the deformable capacitor. The capacitance of the deformable capacitor is given by

$$C(x) = \frac{\varepsilon_0 A}{g + d_0/\varepsilon_r - x} \qquad (2)$$

where ε_0 is the permittivity of free space and ε_r is the relative permittivity of the dielectric layer. In this work we only consider linear capacitors for which the capacitance is equal to the ratio between charge and voltage ($Q = CV$). Also in this work it is assumed that the lateral dimensions of all capacitors are much larger than the nominal gap between the capacitor electrodes. For brevity, the effect of fringing fields is not included in the analysis, though many simplified approximations for specific geometries are available in the literature (e.g. [22]).

The potential of the system may be rewritten in the following normalized form

$$\widetilde{\psi}_Q = \frac{1}{2}\widetilde{x}^2 + \frac{1}{2}(1 + \xi - \widetilde{x})\widetilde{Q}^2 \qquad (3)$$

where

$$\widetilde{\psi}_Q = \frac{\psi_Q}{kg^2}, \quad \widetilde{x} = \frac{x}{g}, \quad \xi = \frac{d_0}{g\varepsilon_r}, \quad \widetilde{Q}^2 = \frac{1}{\varepsilon_0 Akg}Q^2. \qquad (4)$$

The potential is a function of the two state variables of the system $\widetilde{x}$ and $\widetilde{Q}$. The reactive mechanical force that is required to hold the system at any given state is given by the partial derivative of the potential with respect to the mechanical DOF

$$\widetilde{f}_Q = \frac{\partial \widetilde{\psi}_Q}{\partial \widetilde{x}} = \widetilde{x} - \frac{1}{2}\widetilde{Q}^2. \qquad (5)$$

However, the whole point in electrostatic actuation is to drive the movable electrode without applying any external mechanical forces. The condition $\widetilde{f}_Q = 0$ yields the equilibrium state of the system

$$\widetilde{f}_Q = \widetilde{x} - \frac{1}{2}\widetilde{Q}^2 = 0. \qquad (6)$$

The stability of this equilibrium state is determined by the partial derivative of the reactive force with respect to the DOF

$$\widetilde{K}_Q = \frac{\partial \widetilde{f}_Q}{\partial \widetilde{x}} = 1. \qquad (7)$$

The system is stable for $\widetilde{K}_Q > 0$, is unstable for $\widetilde{K}_Q < 0$, and is critically stable for $\widetilde{K}_Q = 0$. Since the stiffness (7) is positive, it follows that the system is always stable. The equilibrium curve of the system is illustrated in Fig. 2.
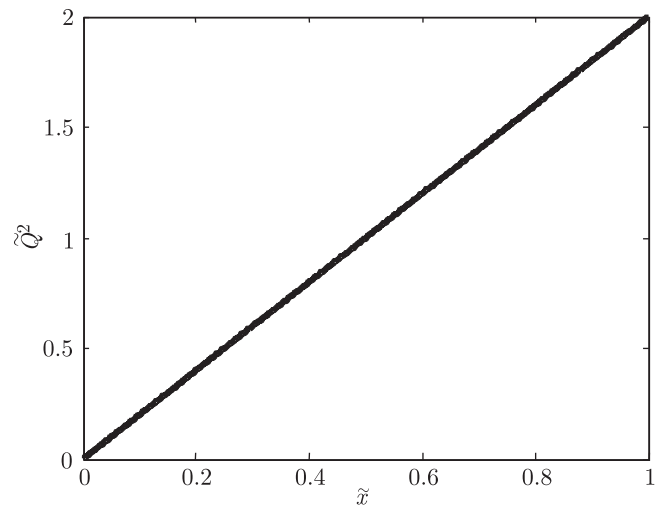

Fig. 2. Equilibrium curve of the charge-driven parallel-plates actuator. The displacement is a monotonic function of charge and the response is stable

When the parallel-plate actuator is driven by voltage, the potential of the voltage source ($\psi_{battery} = -QV$) can be added to the potential of the system to define the *total* potential of the system. The total potential is a function of the two state variables of the system $\widetilde{x}$ and $\widetilde{V}$. The normalized form of the total potential of the system is given by

$$\widetilde{\psi}_V = \frac{1}{2}\widetilde{x}^2 - \frac{1}{2}\frac{\widetilde{V}^2}{1 + \xi - \widetilde{x}} \qquad (8)$$

where

$$\widetilde{\psi}_V = \frac{\psi_V}{kg^2}, \quad \widetilde{V}^2 = \frac{\varepsilon_0 A}{kg^3}V^2. \qquad (9)$$

As before, the reactive mechanical force that is required to hold the system at any given state is the partial derivative of the total potential with respect to the DOF $\widetilde{f}_V = \partial \widetilde{\psi}_V/\partial \widetilde{x}$. The equilibrium state of the system is obtained by setting the mechanical reactive force to zero

$$\widetilde{f}_V = \widetilde{x} - \frac{1}{2}\frac{\widetilde{V}^2}{(1 + \xi - \widetilde{x})^2} = 0. \qquad (10)$$

The stability of this equilibrium state is determined by the partial derivative of the reactive force with respect to the DOF

$$\widetilde{K}_V = \frac{\partial \widetilde{f}_V}{\partial \widetilde{x}} = 1 - \frac{\widetilde{V}^2}{(1 + \xi - \widetilde{x})^3}. \tag{11}$$

The voltage can be extracted from the equilibrium equation (10) and substituted into (11) to yield the stiffness at equilibrium states

$$\widetilde{K}_V = \frac{1 + \xi - 3\widetilde{x}}{1 + \xi - \widetilde{x}}. \tag{12}$$

The system is stable for $\widetilde{K}_V > 0$, is unstable for $\widetilde{K}_V < 0$, and is critically stable for $\widetilde{K}_V = 0$. It follows that the system is stable for $\widetilde{x} < \frac{1}{3}(1 + \xi)$, is unstable for $\widetilde{x} > \frac{1}{3}(1 + \xi)$, and is critically stable at $\widetilde{x} = \frac{1}{3}(1 + \xi)$. The equilibrium curve of the system is illustrated in Fig. 3.
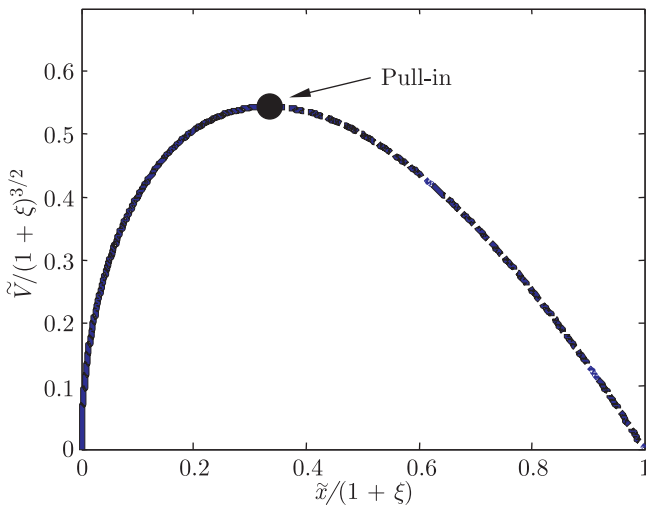

Fig. 3. Equilibrium curve of the voltage-driven parallel-plates actuator. The stable equilibrium (solid) and unstable equilibrium (dashed) coincide at the pull-in state

The displacement of the charge driven actuator is a monotonic function of the applied charge. In contrast, the voltage driven actuator has an equilibrium state only if the applied voltage is lower than the maximal value $\widetilde{V}^2 \leq \frac{8}{27}(1+\xi)^3$. For voltages above this value the system has no equilibrium state and the electrodes of the actuator collapse into contact. The maximal voltage for which equilibrium exists is the Pull-In voltage. For voltages below the pull-in voltage the equilibrium curve has two solutions: a stable solution (solid line in Fig 3) and an unstable solution (dashed line). At the pull-in point, where the voltage is maximal, the stiffness of the system vanishes and the two branches coincide.

For the parallel-plates actuator the pull-in parameters can be derived by setting $\widetilde{K}_V = 0$ in (11) and solving it together with (10) to yield

$$\widetilde{x}_{Spi} = \frac{1}{3}(1 + \xi), \quad \widetilde{V}_{Spi} = \sqrt{\frac{8}{27}}(1 + \xi)^{3/2}. \tag{13}$$

It can be shown that the pull-in state can be derived by any one of the following definitions: 1) where the voltage is maximal along the equilibrium curve, 2) where the stable and unstable branches of the equilibrium coincide, 3) where the stiffness along the equilibrium curve vanishes. It can be shown that all definitions are equivalent [23].

2.2. Static response of the tilt-plate actuator. To demonstrate that pull-in can also occur in electrostatic actuators that are driven by charge, the tilt-plate actuator is next analyzed, using the same methodology as in the previous sub-section. The tilt-plate actuator is schematically illustrated in Fig. 4. This actuator is constructed from a rectangular plate electrode that is suspended on a torsion spring above a fixed bottom electrode. The top electrode has a single angular degree-of-freedom θ, and the stiffness of the spring is k_θ. The bottom electrode is coated with a dielectric layer of thickness d_0 and relative permittivity ε_r. In the unloaded state of the system the top electrode is separated from the dielectric layer by a free-space gap g. The top electrode is subjected to a charge or voltage and the bottom electrode is grounded.

The two electrodes form a deformable capacitor with capacitance

$$C(\theta) = \int_0^L \frac{\varepsilon_0 b}{g + d_0/\varepsilon_r - x\theta} dx$$

$$= -\frac{\varepsilon_0 bL}{g} \frac{1}{\widetilde{\theta}} \ln\left(\frac{1 + \xi - \widetilde{\theta}}{1 + \xi}\right) \tag{14}$$

where b is the plate width, L is its length, and

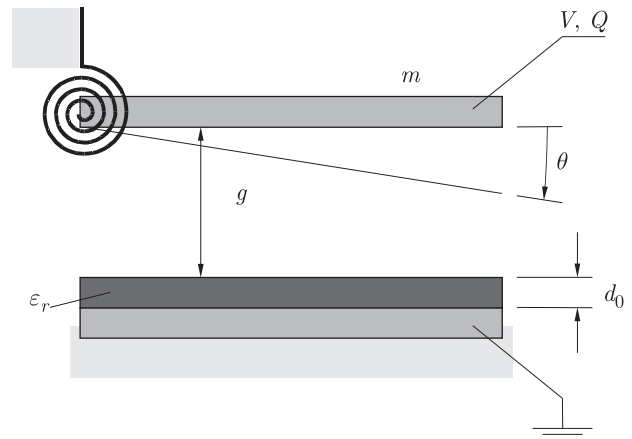$$\widetilde{\theta} = \frac{L}{g}\theta. \tag{15}$$

Fig. 4. Schematic view of the tilt-plate actuator with a dielectric layer coating the bottom electrode

For the charge-driven tilt-plate actuator the potential, equilibrium equation, and stiffness are given by

$$\widetilde{\psi}_Q = \frac{1}{2}\widetilde{\theta}^2 - \frac{1}{2}\widetilde{\theta}\left[\ln\left(\frac{1 + \xi - \widetilde{\theta}}{1 + \xi}\right)\right]^{-1} \widetilde{Q}^2 \tag{16}$$

$$\widetilde{f}_Q = \widetilde{\theta} - \frac{1}{2} \left[\frac{1}{\ln\left(\frac{1+\xi-\widetilde{\theta}}{1+\xi}\right)} \right. \tag{17}$$

$$\left. + \frac{\widetilde{\theta}}{(1+\xi-\widetilde{\theta})\ln\left(\frac{1+\xi-\widetilde{\theta}}{1+\xi}\right)^2} \right] \widetilde{Q}^2 = 0$$

$$\widetilde{K}_Q = 1 - \left[\frac{2\widetilde{\theta} + (2+2\xi-\widetilde{\theta})\ln\left(\frac{1+\xi-\widetilde{\theta}}{1+\xi}\right)}{2(1+\xi-\widetilde{\theta})^2\ln\left(\frac{1+\xi-\widetilde{\theta}}{1+\xi}\right)^3} \right] \widetilde{Q}^2 \tag{18}$$

where

$$\widetilde{\psi}_Q = \frac{L^2}{k_\theta g^2}\psi_Q, \quad \widetilde{Q}^2 = \frac{L}{k_\theta g\varepsilon_0 b}Q^2, \quad \widetilde{f}_Q = \frac{\partial\widetilde{\psi}_Q}{\partial\widetilde{\theta}}, \quad \widetilde{K}_Q = \frac{\partial\widetilde{f}_Q}{\partial\widetilde{\theta}}. \tag{19}$$

The equilibrium states of the system are illustrated in Fig. 5. Even though the actuator is driven by charge, its equilibrium curve shows that there is a limit to the applied charge for which equilibrium can be achieved. Below a critical value of the applied charge, the system has one stable equilibrium state (solid line) and one unstable equilibrium state (dashed line). Above the critical charge the system has no equilibrium state, and at the critical charge the system is critically stable and the two electrodes can spontaneously collapse into contact. This critical state is the static charge-actuation pull-in state, which may be computed by setting $\widetilde{K}_Q = 0$ in (18) and solving it together with (17) to yield

$$\widetilde{\theta}_{Spi} = 0.71065(1+\xi), \quad \widetilde{Q}^2_{Spi} = 1.7977(1+\xi). \tag{20}$$
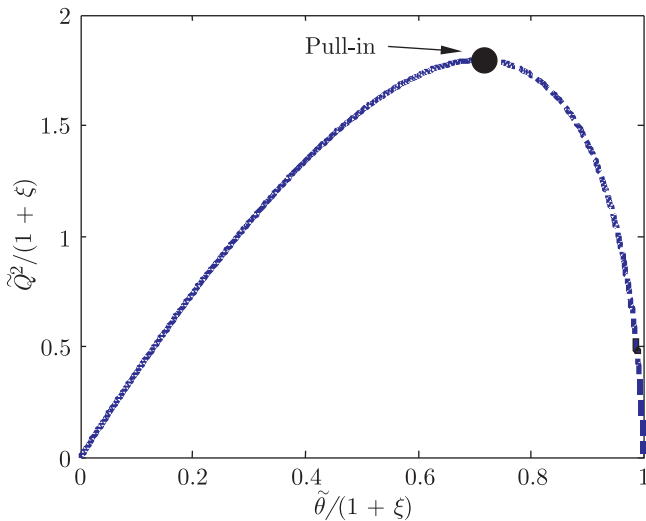

Fig. 5. Equilibrium curve of the charge-driven tilt-plates actuator. The stable equilibrium (solid) and unstable equilibrium (dashed) coincide at the pull-in state

When the tilt-plate actuator is driven by voltage, its total potential, equilibrium equation, and stiffness are given by

$$\widetilde{\psi}_V = \frac{1}{2}\widetilde{\theta}^2 + \frac{1}{2}\frac{1}{\widetilde{\theta}}\ln\left(\frac{1+\xi-\widetilde{\theta}}{1+\xi}\right)\widetilde{V}^2 = 0 \tag{21}$$

$$\widetilde{f}_V = \widetilde{\theta} - \frac{1}{2}\left[\frac{1}{\widetilde{\theta}^2}\ln\left(\frac{1+\xi-\widetilde{\theta}}{1+\xi}\right) + \frac{1}{\widetilde{\theta}(1+\xi-\widetilde{\theta})}\right]\widetilde{V}^2 = 0 \tag{22}$$

$$\widetilde{K}_V = 1 + \left[\frac{1}{\widetilde{\theta}^3}\ln\left(\frac{1+\xi-\widetilde{\theta}}{1+\xi}\right) + \frac{2+2\xi-3\widetilde{\theta}}{2\widetilde{\theta}^2(1+\xi-\widetilde{\theta})^2}\right]\widetilde{V}^2 = 0 \tag{23}$$

where

$$\widetilde{\psi}_V = \frac{L^2}{k_\theta g^2}\psi_V, \quad \widetilde{V}^2 = \frac{\varepsilon_0 bL^3}{k_\theta g^3}V, \quad \widetilde{f}_V = \frac{\partial\widetilde{\psi}_V}{\partial\widetilde{\theta}}, \quad \widetilde{K}_V = \frac{\partial\widetilde{f}_V}{\partial\widetilde{\theta}}. \tag{24}$$

The equilibrium states of the system are illustrated in Fig. 6. This equilibrium curve resembles that of the voltage-driven parallel-plates actuator (Fig. 3). The pull-in state can be computed by setting $\widetilde{K}_V = 0$ in (23) and solving it together with (22) to yield

$$\widetilde{\theta}_{Spi} = 0.44042(1+\xi), \quad \widetilde{V}^2_{Spi} = 0.82745(1+\xi)^3. \tag{25}$$
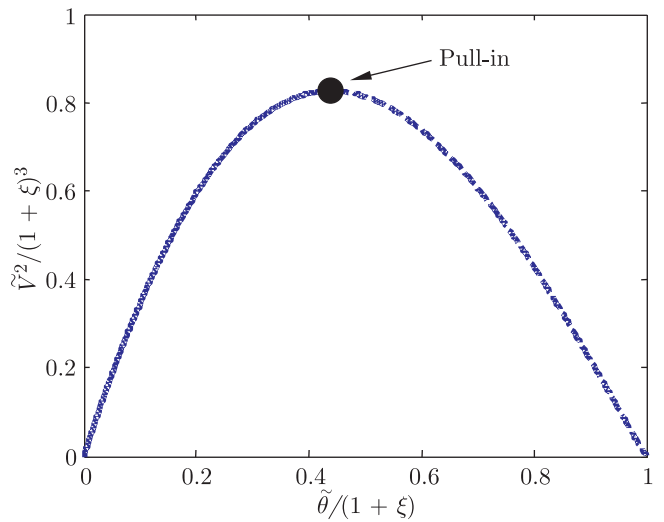

Fig. 6. Equilibrium curve of the voltage-driven tilt-plates actuator

In the charge-driven parallel-plates actuator pull in does not occur because the electrostatic force is proportional to the charge which is uniformly distributed over the electrodes (the effect of fringing fields is not considered in this work). In contrast, the electrostatic moment that drives the tilt-plate actuator is affected not only by the applied charge but also by the charge distribution over the electrodes. The charge pull-in instability results from charge redistribution. As charge is increased the tilt angle increases and a larger portion of the charge concentrates in regions where the actual gap is smaller (i.e. farther away from the axis of rotation). This charge concentration becomes unstable as the pull-in charge is approached.

Though many electrostatic actuators are modelled as effective parallel-plates (e.g. [24]), in many actuators (e.g. the clamped-clamped beam actuator [25]) the charge distribution is far from being uniform, and charge pull-in may occur. This is demonstrated on the clamped-clamped beam actuator in the next sub-section.

2.3. Static response of the clamped-clamped beam actuator. RF-MEMS is an important emerging field, and currently promising applications in this field are Ohmic and capacitive micro-switches [8,10,11]. In these electrostatic switches the pull-in instability is utilized to achieve rapid transition between two states of the system. Efficient modelling tools that can accurately predict the pull-in parameters of electrostatic switches are required to ensure a successful design.

In this sub-section, the static response of a charge-driven and a voltage-driven clamped-clamped beam actuator is analyzed. A schematic view of the clamped-clamped beam actuator is presented in Fig. 7. The deformable bridge structure is clamped on both edges and is suspended over a fixed Co-Planar Wave-guide (CPW [8]). The central bottom electrode (i.e. the line of the CPW) is coated by a dielectric layer and serves as the driving electrode.

The clamped-clamped beam actuator may not be modelled as a single DOF system. Due to the nonlinear nature of electrostatic forces and additional nonlinear effects, simulation of the electromechanical response of this system requires the use of numerical computation of approximate solutions. In this section a strategy for increasing the efficiency of the numerical computation is presented. It is simpler to first consider the response of the voltage-driven system. Once the response of the voltage-driven system has been derived, the response of the charge-driven system can be obtained at a small additional effort. Therefore, from this point on, for all systems, voltage actuation will be considered before charge actuation.

The equilibrium equation of the voltage driven clamped-clamped beam actuator is given by

$$E^* I \frac{d^4 y}{dx^4} - EA \left[\frac{1}{L} \int_0^L \frac{1}{2} \left(\frac{dy}{dx} \right)^2 dx \right] \frac{d^2 y}{dx^2} = f_E \quad (26)$$

where

$$f_E = \begin{cases} 0 & \text{for} & 0 < x < (1-\alpha)L/2 \\ \frac{1}{2} \frac{\varepsilon_0 b V^2}{(g + d_0/\varepsilon_r - y)^2} & \text{for } (1-\alpha)L/2 \leq x \leq (1+\alpha)L/2 \\ 0 & \text{for} & (1+\alpha)L/2 < x < L \end{cases}. \quad (27)$$

Here $y(x)$ is the deflection of the beam and x is the coordinate along the beam axis, E^* is the effective elastic modulus in bending, $I = bh^3/12$ is the second moment of the beam cross-section where b and h are the cross-section width and height, E is the Young modulus of the beam material, A is the cross-section area, L is the beam length and g is the nominal gap between the electrodes. For a thin beam (i.e. $h \ll b$) the effective elastic modulus in bending is given by $E^* = E/(1-\nu^2)$ where ν is the Poisson ratio.

The three terms in (26) are the distributed forces due to: bending, membrane stress stiffening, and electrostatic attraction. The normalized form of the equilibrium equation is given by

$$\frac{d^4 \widetilde{y}}{d\widetilde{x}^4} - 6 \frac{E}{E^*} \widetilde{g}^2 \left[\int_0^1 \left(\frac{d\widetilde{y}}{d\widetilde{x}} \right)^2 d\widetilde{x} \right] \frac{d^2 \widetilde{y}}{d\widetilde{x}^2} = \widetilde{f}_E \quad (28)$$

where

$$\widetilde{f}_E = \begin{cases} 0 & \text{for} & 0 < \widetilde{x} < (1-\alpha)/2 \\ \frac{\widetilde{V}^2}{(1 + \xi - \widetilde{y})^2} & \text{for } (1-\alpha)/2 \leq \widetilde{x} \leq (1+\alpha)/2 \\ 0 & \text{for} & (1+\alpha)/2 < \widetilde{x} < 1 \end{cases} \quad (29)$$

and

$$\widetilde{x} = \frac{x}{L}, \ \widetilde{y} = \frac{y}{g}, \ \widetilde{g} = \frac{g}{h}, \ \widetilde{E} = \frac{E}{E^*}, \ \widetilde{V}^2 = \frac{\varepsilon_0 b L^4}{2 E^* g^3 I} V^2. \quad (30)$$

The nonlinear equilibrium equation (28) can be solved numerically for a given value of applied voltage. By iteratively increasing the applied voltage and ensuring that the solution converges to a stable equilibrium, the pull-in state may be approached. However, as the pull-in voltage is approached and the system becomes unstable, the convergence of the numerical solution vanishes [25]. Therefore, extraction of the pull-in parameters with reasonable accuracy will require a very long computation time.

Recently an efficient algorithm for extracting the pull-in parameters was proposed [25]. This algorithm is based on displacement iterations rather than voltage iterations. In the following, a simplified form of this algorithm is presented.
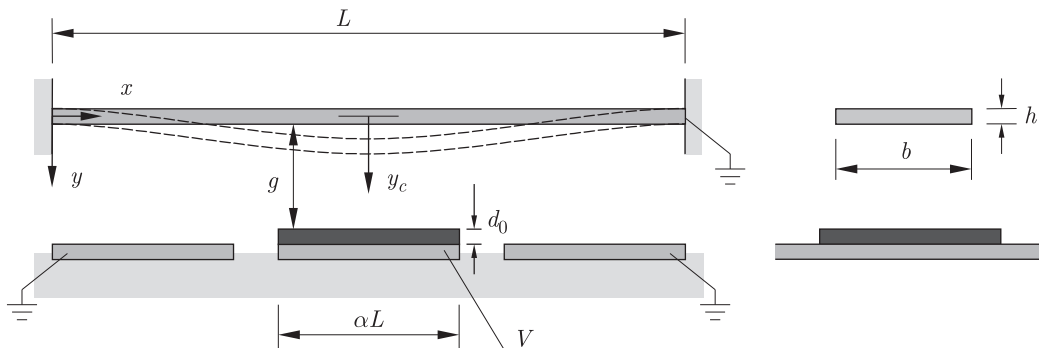

Fig. 7. Schematic view of a typical RF-MEMS capacitive switch showing the clamped-clamped beam actuator with geometrical details of the cross-section. The switch is driven by the central bottom electrode which is coated by a dielectric insulator

In the displacement iteration approach, the displacement of a pre-chosen point in the system is postulated. For example, the deflection y_c of the beam centre (Fig. 7) may be arbitrarily set to any value in the range $0 < \widetilde{y}_c < 1$. A simple computation of the equilibrium state (when no voltage is applied) will yield the mechanical reactive force that is required to maintain the subscribed deflection at this point. Then, for each postulated value of y_c, the value of the applied voltage that nullifies this reactive force may be computed. The resulting equilibrium state is stable because the deflection $\widetilde{y}_c$ is fixed. However, since the clamped-clamped beam is only subjected to an electrostatic force and the reactive force at the pre-chosen point is zero, this equilibrium state is also an equilibrium state of the original problem.

In the displacement iterations approach, equivalent problems in which the deflection of a pre-chosen point is iterated are solved instead of solving the voltage-driven system. Each of the equivalent problems is stable and therefore the displacement-iteration computation rapidly converges to all equilibrium states of the voltage-driven system (both stable and unstable) [25].

Figure 8 presents the equilibrium curve of the voltage-driven clamped-clamped beam actuator, for $\widetilde{g} \ll 1$, $\widetilde{E} = 1$, $\xi = 0.01$ and $\alpha = 0.3$. The pull-in parameters of the voltage-driven clamped-clamped beam actuator are found to be

$$\widetilde{y}_{c\,Spi} = 0.358, \quad \widetilde{V}_{Spi} = 10.617. \tag{31}$$

For any of the given states, the normalized capacitance of the system can be readily computed by

$$\widetilde{C} = \int\limits_{\widetilde{x}=(1-\alpha)/2}^{(1+\alpha)/2} \frac{1}{1+\xi-\widetilde{y}} d\widetilde{x}. \tag{32}$$

Then, for any equilibrium state the normalized charge is given by

$$\widetilde{Q} = \widetilde{C}\widetilde{V} \tag{33}$$

where

$$\widetilde{Q}^2 = \frac{1}{2}\frac{L^4}{\varepsilon_0 bE^* Ig}Q^2. \tag{34}$$

The displacement iteration enables to compute the entire equilibrium curve of the voltage-driven actuator (stable and unstable alike). Once this has been done, it is quite easy to compute the charge associated with each equilibrium state, and at a negligible computational effort, obtain the equilibrium curve of the charge-driven actuator.

Figure 8 presents the equilibrium curve of the voltage-driven clamped-clamped beam actuator, for the case $\widetilde{g} \ll 1$, $\xi = 0.01$ and $\alpha = 0.3$. The pull-in parameters of the charge-driven clamped-clamped beam actuator are found to be

$$\widetilde{y}_{c\,Spi} = 0.892, \quad \widetilde{Q}_{Spi} = 7.056. \tag{35}$$

The electromechanical response of the clamped-clamped beam actuator with a central electrode ($\alpha = 0.3$) may seem rather similar to that of the parallel-plates actuator. However, the response under charge actuation reveals that charge distribution is not uniform (as may be expected), and that charge pull-in may occur.
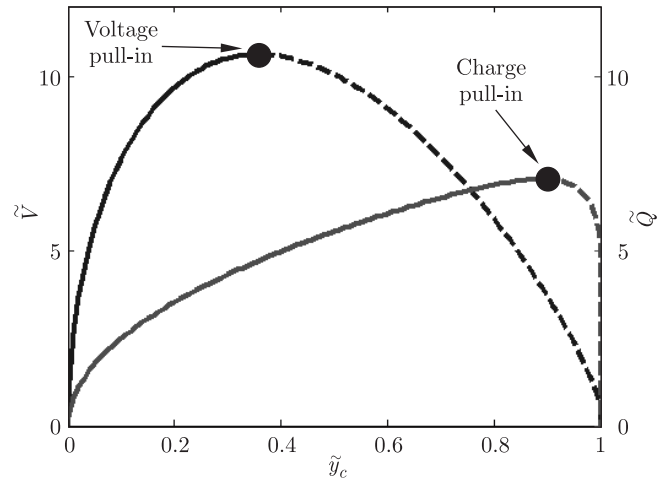

Fig. 8. Equilibrium curve of the charge-driven and voltage-driven clamped-clamped beam actuator (for $\widetilde{g} \ll 1$, $\widetilde{E} = 1$, $\xi = 0.01$ and $\alpha = 0.3$)

3. Dynamic response of electrostatic actuators

The analysis presented in the previous section is often used to design electrostatic switches. However, the response of electrostatic switches is far from being quasi-static, and the effect of inertial forces must be considered. The most common way of driving electrostatic switches is subjecting them to a step-function of charge or voltage, when they are at rest in the unloaded state. In this study we only consider actuators in which damping forces are negligible. This allows us to consider the shortest switching time and the lowest values of charge or voltage that are sufficient to achieve a switching response. The effect of damping is predictable in the sense that it slows the dynamic response and makes it closer to the quasi-static response considered earlier.

In this section we are specifically interested in the pull-in instability within the context of a dynamic response. In this section we present a method for estimating the dynamic response of un-damped electromechanical systems in which we only consider static states of the system. This method yields exact results in the case of systems with a single DOF, and yields an approximation of the pull-in state in the case of actuator with more than one DOF. For brevity, this method is henceforth referred to by its acronym DRAUSS which stands for Dynamic Response Analysis Using Static States.

3.1. Dynamic response of the parallel-plates actuator.
Now, we consider the un-damped dynamic response of the parallel-plate actuator illustrated in Fig. 1. The dynamic response of the actuator when it is subjected to a step-function voltage, is derived from the Hamiltonian of the system given by [18]

$$H_V = \frac{1}{2}m\dot{x}^2 + \frac{1}{2}kx^2 - \frac{\varepsilon_0 A}{2\left(g+\frac{d_0}{\varepsilon_r}-x\right)}V^2 \tag{36}$$

where m is the mass of the movable electrode and $\dot{x}$ is its velocity. The Hamiltonian is the sum of the kinetic energy, the elastic potential of the suspension, and the electrostatic potential of the deformable capacitor and of the voltage source.

The Hamiltonian may be rewritten in the normalized form

$$\widetilde{H}_V = \frac{1}{2}\dot{\widetilde{x}}^2 + \frac{1}{2}\widetilde{x}^2 - \frac{1}{2}\frac{\widetilde{V}^2}{1+\xi-\widetilde{x}} \qquad (37)$$

where

$$\widetilde{H}_V = \frac{H_V}{kg^2}, \quad \widetilde{t} = \sqrt{\frac{k}{m}}t, \quad \dot{\widetilde{x}} = \frac{d\widetilde{x}}{d\widetilde{t}}. \qquad (38)$$

The location of the movable electrode as a function of time can be computed from the momentum equation that is derived from the Hamiltonian in the form

$$\ddot{\widetilde{x}} = -\frac{\partial \widetilde{H}}{\partial \widetilde{x}} = -\widetilde{x} + \frac{1}{2}\frac{\widetilde{V}^2}{(1+\xi-\widetilde{x})^2} \qquad (39)$$

where

$$\ddot{\widetilde{x}} = \frac{d^2\widetilde{x}}{d\widetilde{t}^2}. \qquad (40)$$

The momentum equation (39) can be integrated twice in time to find the displacement of the electrode as a function of time $\widetilde{x}(\widetilde{t})$. Figure 9 illustrates the trajectory of the top electrode for several values of applied voltage. These simulation results were obtained by numerical time-integration of (39) using MATLAB®.
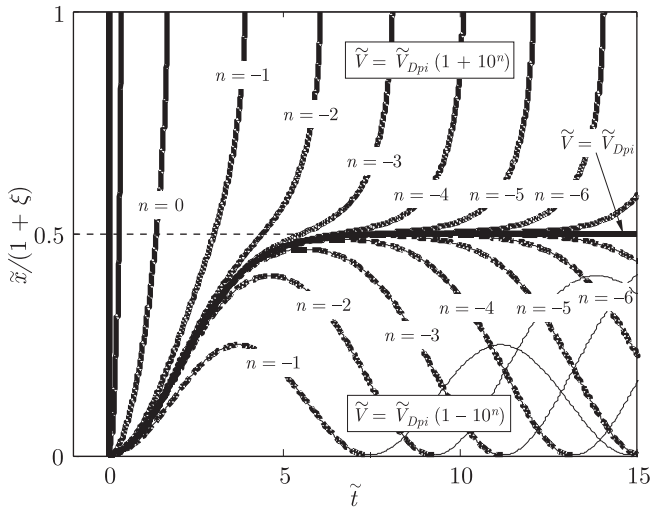

Fig. 9. Dynamic response of the voltage-driven parallel-plates actuator for various values of applied voltage. For voltages below the dynamic pull-in voltage $\widetilde{V} = \widetilde{V}_{Dpi}$ the response is periodic (dashed lines) and for voltages above this critical value the response is non-periodic (solid)

Below a critical value of the applied voltage, the dynamic response of the actuator is periodic. For voltages above this critical value, the response is non-periodic, the velocity of the movable electrode is always positive, and it eventually collapses into contact with the fixed electrode. When the critical voltage is applied, the movable electrode converges to an unstable equilibrium state [18]. This critical dynamic state is the

Dynamic Pull-in state of the system and it can be computed by using the DRAUSS method described in the following.

In this work damping is neglected and accordingly, once the voltage is applied (at $\widetilde{t} = 0$ when $\widetilde{x} = 0$ and $\dot{\widetilde{x}} = 0$), the Hamiltonian is unchanged ($\widetilde{H}_{\widetilde{V}} = \widetilde{H}_{\widetilde{V}(\widetilde{t}=0)}$). Setting $\widetilde{H}_{\widetilde{V}(\widetilde{t}=0)} = -\widetilde{V}^2/(1+\xi)/2$ results in an energy constraint on the dynamic response, as formulated by the following dynamic response function

$$D_{\widetilde{V}} = \frac{1}{2}\dot{\widetilde{x}}^2 + \frac{1}{2}\widetilde{x}^2 - \frac{1}{2}\widetilde{V}^2\frac{\widetilde{x}}{(1+\xi-\widetilde{x})(1+\xi)} = 0. \quad (41)$$

The dynamic pull-in state of the parallel-plates actuator is a stagnation state which can be computed by setting $\dot{\widetilde{x}} = 0$ in (41) to yield the stagnation curve of the system

$$S_{\widetilde{V}} = \frac{1}{2}\widetilde{x}^2 - \frac{1}{2}\widetilde{V}^2\frac{\widetilde{x}}{(1+\xi-\widetilde{x})(1+\xi)} = 0. \qquad (42)$$

The solution of (42) yields the stagnation displacements for a given value of $\widetilde{V}$. The three solutions of (42) are

$$\widetilde{x}_I = 0 \qquad (43)$$

$$\widetilde{x}_{II} = \frac{(1+\xi)^2 - \sqrt{(1+\xi)^4 - 4(1+\xi)\widetilde{V}^2}}{2(1+\xi)} \qquad (44)$$

$$\widetilde{x}_{III} = \frac{(1+\xi)^2 + \sqrt{(1+\xi)^4 - 4(1+\xi)\widetilde{V}^2}}{2(1+\xi)}. \qquad (45)$$

The first solution is the trivial solution (solid line at the origin in Fig. 10); the second solution is a physical branch of the stagnation curve (thick solid), and the third solution is the unphysical branch (thick dashed). The physical and unphysical stagnation states coalesce when $\sqrt{(1+\xi)^4 - 4(1+\xi)\widetilde{V}^2} = 0$. At this point the stagnation curve and the equilibrium curve intersect, and the voltage along the stagnation curve is maximal.
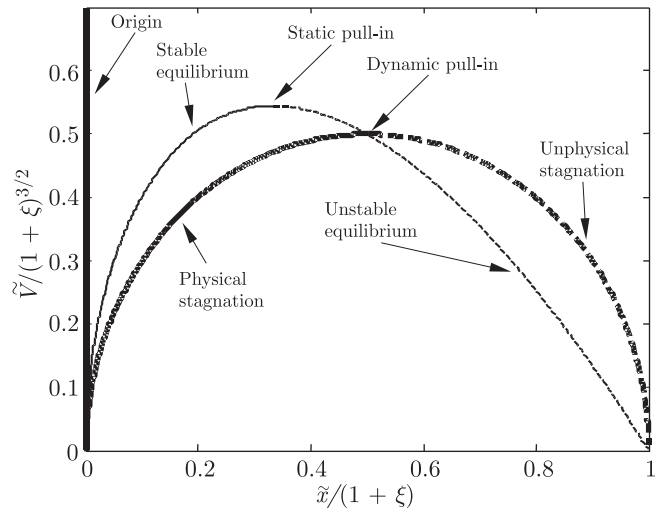

Fig. 10. Equilibrium (thin lines) and stagnation (thick lines) curves of the voltage-driven parallel-plates actuator

Accordingly, the dynamic pull-in state of the parallel-plates actuator is found to be

$$\widetilde{x}_{Dpi} = \frac{1}{2}(1+\xi), \quad \widetilde{V}_{Dpi} = \frac{1}{2}(1+\xi)^{3/2}. \qquad (46)$$

The dynamic pull-in point can be computed in one of three equivalent ways [18]: 1) The point of maximal voltage along the stagnation curve. 2) The point where the physical and unphysical branches of the stagnation curve coalesce. 3) The intersection point of the equilibrium and stagnation curves.

The presented method of analysis is computationally efficient because it only considers static states.

When the parallel-plates actuator is driven from its unloaded state by application of a step-function of charge, the Hamiltonian of the system is given by

$$H_Q = \frac{1}{2}m\dot{x}^2 + \frac{1}{2}kx^2 + \frac{g + \frac{d_0}{\varepsilon_r} - x}{2\varepsilon_0 A}Q^2. \qquad (47)$$

The last term on the right hand side of (47) is the electrostatic potential of the deformable capacitor. The Hamiltonian may be rewritten in the normalized form

$$\widetilde{H}_Q = \frac{1}{2}\dot{\widetilde{x}}^2 + \frac{1}{2}\widetilde{x}^2 + \frac{1}{2}(1 + \xi - \widetilde{x})\widetilde{Q}^2 \qquad (48)$$

where $\widetilde{Q}$ is given in (24). Once the charge is applied (at $\tilde{t} = 0$ when $\widetilde{x} = 0$ and $\dot{\widetilde{x}} = 0$), the Hamiltonian is unchanged. Setting $\widetilde{H}_Q = \widetilde{H}_{Q(\tilde{t}=0)} = (1 + \xi)\widetilde{Q}^2$ yields an energy constraint on the dynamic response as formulated by the following dynamic response function

$$D_Q = \frac{1}{2}\dot{\widetilde{x}}^2 + \frac{1}{2}\widetilde{x}^2 - \frac{1}{2}\widetilde{x}\widetilde{Q}^2 = 0. \qquad (49)$$

The momentum equation that describes the motion of the top electrode may be derived from the Hamiltonian in the form

$$\ddot{\widetilde{x}} = \frac{\partial \widetilde{H}}{\partial \widetilde{x}} = -\widetilde{x} + \frac{1}{2}\widetilde{Q}^2. \qquad (50)$$

The solution of this momentum equation is

$$\widetilde{x} = \frac{1}{2}(1 - \cos(\tilde{t}))\widetilde{Q}^2. \qquad (51)$$

This is a harmonic oscillation about the static equilibrium state $\widetilde{x} = \frac{1}{2}\widetilde{Q}^2$. It follows that the dynamic response of the charge-driven parallel-plates actuator is a stable periodic response for which the amplitude is a monotonically increasing function of the applied charge.

3.2. Dynamic response of the tilt-plate actuator. The dynamic electromechanical response of the tilt-plate actuator when it is driven by a step-function of voltage, is derived from the Hamiltonian given by

$$H_V = \frac{1}{2}I\dot{\theta} + \frac{1}{2}k_\theta\theta^2 - \frac{1}{2}CV^2 = -\frac{1}{2}C_{(\theta=0)}V^2. \qquad (52)$$

The first term on the left hand side of (52) is the kinetic energy of the top plate-electrode where I is its moment of inertia and the other two terms are the total potential of the actuator. As damping is ignored, once the step-function voltage is applied, the Hamiltonian remains unchanged (right-hand side of (52)).

The normalized form of the Hamiltonian is given by

$$\widetilde{H}_V = \frac{1}{2}\dot{\widetilde{\theta}}^2 + \frac{1}{2}\widetilde{\theta}^2 + \frac{1}{2}\frac{1}{\widetilde{\theta}}\ln\left(\frac{1 + \xi - \widetilde{\theta}}{1 + \xi}\right)\widetilde{V}^2 = -\frac{1}{2}\frac{1}{1 + \xi}\widetilde{V}^2 \qquad (53)$$

where

$$\dot{\widetilde{\theta}} = \frac{d\widetilde{\theta}}{d\tilde{t}}, \quad \tilde{t} = \sqrt{\frac{k_\theta}{I}}t. \qquad (54)$$

The equation of motion can be derived from the Hamiltonian in the form

$$\ddot{\widetilde{\theta}} = \frac{\partial \widetilde{H}}{\partial \widetilde{\theta}} = -\widetilde{\theta} + \frac{\widetilde{V}^2}{2\widetilde{\theta}}\left[\frac{1}{\widetilde{\theta}}\ln\left(\frac{1 + \xi - \widetilde{\theta}}{1 + \xi}\right) + \frac{1}{1 + \xi - \widetilde{\theta}}\right]. \qquad (55)$$

The dynamic response of the tilt-plate actuator, for various applied voltages is illustrated in Fig. 11. Below a critical value of the step-function voltage the response is periodic (dashed lines), and for voltages that are higher than this critical value the response is a-periodic (solid lines) and the top electrode impacts the bottom electrode. The critical value of the applied voltage is the dynamic pull-in voltage. When the dynamic pull-in voltage is applied, the top electrode reaches a stagnation state that separates the periodic and a-periodic responses.
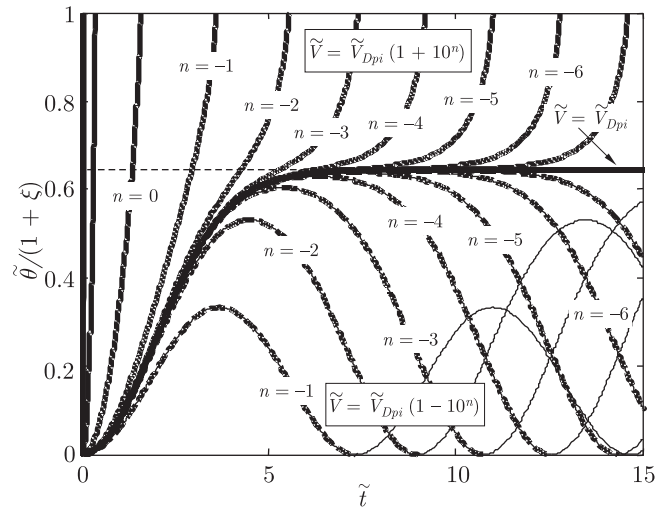

Fig. 11. Dynamic response of the voltage-driven tilt-plate actuator for various values of applied voltage. For voltages below the dynamic pull-in voltage the response $\widetilde{V} = \widetilde{V}_{Dpi}$ is periodic (dashed lines) and for voltages above this critical value the response is non-periodic (solid)

The dynamic pull-in voltage is derived from the dynamic response function which is obtained from (53) by collecting all terms on one side of the equation.

$$D_V = \frac{1}{2}\dot{\widetilde{\theta}}^2 + \frac{1}{2}\widetilde{\theta}^2 + \frac{1}{2}\left[\frac{1}{\widetilde{\theta}}\ln\left(\frac{1 + \xi - \widetilde{\theta}}{1 + \xi}\right) + \frac{1}{1 + \xi}\right]\widetilde{V}^2 = 0. \qquad (56)$$

In the periodic response, the top electrode has stagnation states in which the velocity of the top plate vanishes. To this end, the stagnation function is derived by setting $\dot{\widetilde{\theta}} = 0$ in (56)

$$S_V = \frac{1}{2}\widetilde{\theta}^2 + \frac{1}{2}\left[\frac{1}{\widetilde{\theta}}\ln\left(\frac{1 + \xi - \widetilde{\theta}}{1 + \xi}\right) + \frac{1}{1 + \xi}\right]\widetilde{V}^2 = 0. \quad (57)$$

The stagnation function relates the stagnation tilt angle and the applied voltage. The stagnation curve is illustrated in Fig. 12

where thick solid lines mark the origin and physical stagnation states, and the thick dashed line marks the unphysical branch of the stagnation function. To compute the point where the stagnation and equilibrium curves intersect, the voltage is extracted from (22) and substituted into (57). The solution of the resulting equation is

$$\widetilde{\theta}_{Dpi} = 0.64501(1 + \xi), \quad \widetilde{V}_{Dpi}^2 = 0.68692(1 + \xi)^3. \quad (58)$$
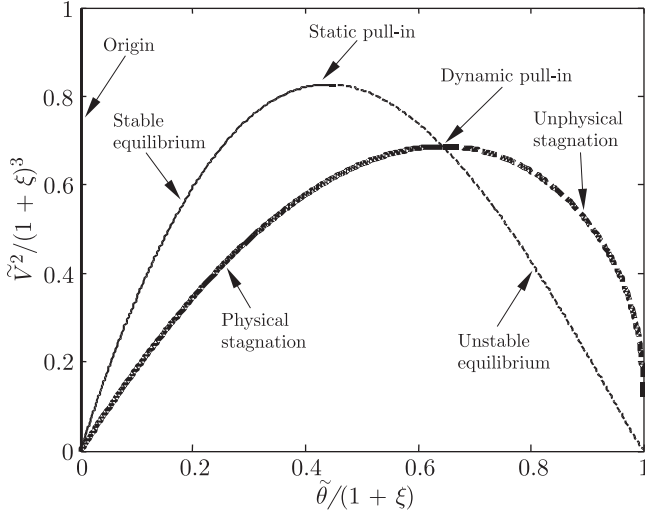

Fig. 12. Equilibrium (thin lines) and stagnation (thick lines) curves of the voltage-driven tilt-plates actuator

When the tilt-plate actuator is driven from its unloaded state by application of a step-function of charge, the Hamiltonian of the system is given by

$$H_Q = \frac{1}{2} I \dot{\theta}^2 + \frac{1}{2} k_\theta \theta^2 + \frac{1}{2} \frac{Q^2}{C(\theta)} = \frac{1}{2} \frac{Q^2}{C(0)}. \quad (59)$$

Once the step-function of charge is applied, the Hamiltonian remains unchanged (right-hand side of (59)). The normalized form of the Hamiltonian is given by

$$\widetilde{H}_Q = \frac{1}{2} \dot{\widetilde{\theta}}^2 + \frac{1}{2} \widetilde{\theta}^2 - \frac{1}{2} \widetilde{\theta} \left[\ln \left(\frac{1 + \xi - \widetilde{\theta}}{1 + \xi} \right) \right]^{-1} \widetilde{Q}^2$$
$$= \frac{1}{2} (1 + \xi) \widetilde{Q}^2 \quad (60)$$

where $\dot{\widetilde{\theta}}$ and $\widetilde{t}$ are defined in (54). The equation of motion can be derived from the Hamiltonian in the form

$$\ddot{\widetilde{\theta}} = -\frac{\partial \widetilde{H}}{\partial \widetilde{\theta}}$$
$$= -\widetilde{\theta} + \frac{1}{2} \left[\frac{1}{\ln \left(\frac{1 + \xi - \widetilde{\theta}}{1 + \xi} \right)} + \frac{\widetilde{\theta}}{(1 + \xi - \widetilde{\theta}) \ln \left(\frac{1 + \xi - \widetilde{\theta}}{1 + \xi} \right)^2} \right] \widetilde{Q}^2. \quad (61)$$

The dynamic response of the tilt-plate actuator, for various applied charges is illustrated in Fig. 13. Below a critical value of the step-function charge, the response is periodic, and for charges that are higher than this critical value, the response is

a-periodic and the top electrode impacts the bottom electrode. The critical value of the applied charge is the dynamic pull-in charge. When the dynamic pull-in charge is applied, the top electrode reaches a stagnation state that separates the periodic and a-periodic responses.
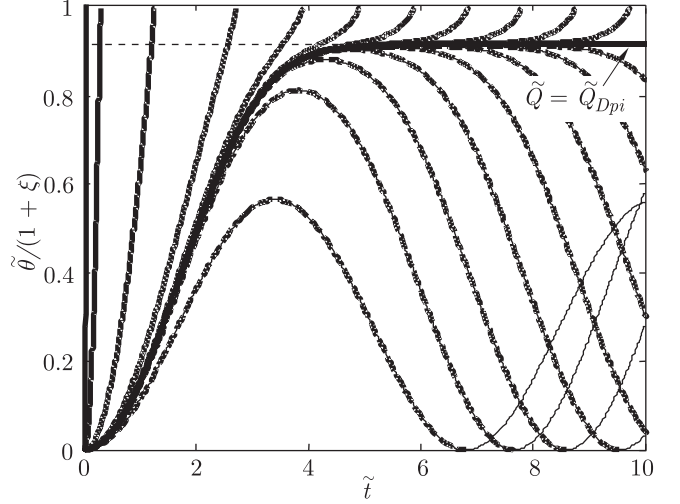

Fig. 13. Dynamic response of the charge-driven tilt-plate actuator for various values of applied charge. For charges below the dynamic pull-in charge $\widetilde{Q} = \widetilde{Q}_{Dpi}$ the response is periodic (dashed lines) and for voltages above this critical value the response is non-periodic (solid)

The dynamic response function of the actuator is given by

$$D_Q = \frac{1}{2} \dot{\widetilde{\theta}}^2 + \frac{1}{2} \widetilde{\theta}^2$$
$$- \frac{1}{2} \left\{ \widetilde{\theta} \left[\ln \left(\frac{1 + \xi - \widetilde{\theta}}{1 + \xi} \right) \right]^{-1} + (1 + \xi) \right\} \widetilde{Q}^2 = 0. \quad (62)$$

The stagnation function is derived by setting $\dot{\widetilde{\theta}} = 0$ in (62)

$$S_Q = \frac{1}{2} \widetilde{\theta}^2$$
$$- \frac{1}{2} \left\{ \widetilde{\theta} \left[\ln \left(\frac{1 + \xi - \widetilde{\theta}}{1 + \xi} \right) \right]^{-1} + (1 + \xi) \right\} \widetilde{Q}^2 = 0. \quad (63)$$

The stagnation function relates the stagnation tilt angle and the applied charge. The stagnation curve is illustrated in Fig. 14, where thick solid lines mark the origin and physical stagnation states, and the thick dashed line marks the unphysical branch of the stagnation function.

To compute the point where the stagnation and equilibrium curves intersect, charge is extracted from (17) and substituted into (63). The solution of the resulting equation is

$$\widetilde{\theta}_{Dpi} = 0.91635(1 + \xi), \quad \widetilde{Q}_{Dpi}^2 = 1.3314(1 + \xi). \quad (64)$$
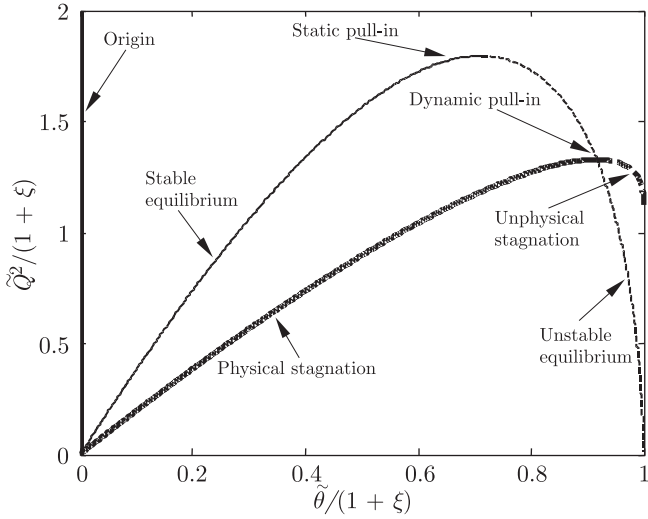
Fig. 14. Equilibrium (thin lines) and stagnation (thick lines) curves of the charge-driven tilt-plates actuator

3.3. Dynamic response of the clamped-clamped beam actuator.

In this sub-section we analyze the dynamic response of a more realistic model of an electrostatic switch. The normalized form of the equation of motion of the voltage-driven clamped-clamped beam actuator is given by

$$\frac{\partial^2 \widetilde{y}}{\partial \widetilde{t}^2} = -\frac{\partial^4 \widetilde{y}}{\partial \widetilde{x}^4} + 6\widetilde{E}\widetilde{g}^2 \left[\int_0^1 \left(\frac{\partial \widetilde{y}}{\partial \widetilde{x}} \right)^2 d\widetilde{x} \right] \frac{\partial^2 \widetilde{y}}{\partial \widetilde{x}^2} + \widetilde{f}_E \quad (65)$$

where $\widetilde{f}_E$ is given by (29), $\tilde{t} = \sqrt{\frac{E^*I}{\gamma L^4}}t$, and the other normalized variables are given by (30). The initial and boundary conditions of the system are

$$\widetilde{y} = \frac{d\widetilde{y}}{d\widetilde{t}} = 0 \qquad \text{for } \tilde{t} = 0$$
$$\widetilde{y} = \frac{d\widetilde{y}}{d\widetilde{x}} = 0 \quad \text{at } \widetilde{x} = 0 \text{ and } \widetilde{x} = 1. \quad (66)$$

The equation of motion may be numerically integrated in time to compute the displacement as function of time. Figure 15 illustrates the trajectory of the beam center for several values of the applied voltage (for $\widetilde{g} \ll 1$, $\widetilde{E} = 1$, $\xi = 0.01$ and $\alpha = 0.3$).

This figure resembles the dynamic response of the parallel-plates actuator presented in Fig. 9. The waviness that may be observed in the trajectory curves is due to higher-mode vibrations of the continuous beam. To extract the dynamic pull-in voltage, many simulation of the time response are executed. From this time integration it is found that the dynamic pull-in voltage of the system is $\widetilde{V}_{Dpi} = 9.745$.

Next, we compute the dynamic pull-in voltage using the DRAUSS approach. The normalized form of the Hamiltonian of the system is given by

$$\widetilde{H}_V = \frac{1}{2} \int_0^1 \left(\frac{d\widetilde{y}}{d\widetilde{t}} \right)^2 d\widetilde{x} + \frac{1}{2} \int_0^1 \left(\frac{d^2\widetilde{y}}{d\widetilde{x}^2} \right)^2 d\widetilde{x}$$

$$+6\widetilde{E}\widetilde{g}^2 \left[\int_0^1 \frac{1}{2} \left(\frac{d\widetilde{y}}{d\widetilde{x}} \right)^2 d\widetilde{x} \right]^2$$
$$-\widetilde{V}^2 \int_{(1-\alpha)/2}^{(1+\alpha)/2} \frac{1}{1+\xi-\widetilde{y}} d\widetilde{x} \quad (67)$$

where

$$\widetilde{H} = \frac{L^3}{E^*Ig^2}H. \quad (68)$$

The normalized forms of the dynamic response function and of the stagnation function, are given by

$$\widetilde{D}_V = \frac{1}{2} \int_0^1 \left(\frac{d\widetilde{y}}{d\widetilde{t}} \right)^2 d\widetilde{x} + \frac{1}{2} \int_0^1 \left(\frac{d^2\widetilde{y}}{d\widetilde{x}^2} \right)^2 d\widetilde{x}$$

$$+6\widetilde{E}\widetilde{g}^2 \left[\int_0^1 \frac{1}{2} \left(\frac{d\widetilde{y}}{d\widetilde{x}} \right)^2 d\widetilde{x} \right]^2$$

$$-\widetilde{V}^2 \int_{(1-\alpha)/2}^{(1+\alpha)/2} \frac{\widetilde{y}}{(1+\xi)(1+\xi-\widetilde{y})} d\widetilde{x} = 0 \quad (69)$$

$$\widetilde{S}_V = \frac{1}{2} \int_0^1 \left(\frac{d^2\widetilde{y}}{d\widetilde{x}^2} \right)^2 d\widetilde{x} + 6\widetilde{E}\widetilde{g}^2 \left[\int_0^1 \frac{1}{2} \left(\frac{d\widetilde{y}}{d\widetilde{x}} \right)^2 d\widetilde{x} \right]^2$$

$$-\widetilde{V}^2 \int_{(1-\alpha)/2}^{(1+\alpha)/2} \frac{\widetilde{y}}{(1+\xi)(1+\xi-\widetilde{y})} d\widetilde{x} = 0. \quad (70)$$

Figure 16 presents the equilibrium and stagnation curves of the system. The dynamic pull-in voltage at the intersection of the equilibrium and stagnation curves is $\widetilde{V}_{Dpi} = 9.741$ (a 0.04% error relative to the value extracted from time integration).

In a similar fashion, the dynamic pull-in charge of the clamped-clamped beam actuator may be computed. For the actuator with the considered geometry the dynamic pull-in charge computed by the DRAUSS approach will also be very close to the value computed by time integration.

The reason that the values computed by the two methods are so close, is that the electrode extension is limited to the central section of the beam, $\alpha = 0.3$. Therefore, the beam response is rather close to a single DOF parallel-plates actuator. For a wider electrode extension, the difference between the two computation methods may be larger. In any case, it has been shown that the dynamic pull-in voltage computed by the DRAUSS approach is a lower bound for the value that is extracted by time integration [18].

To emphasize the advantage of the DRAUSS approach, it is noted that each time integration trajectory presented in Fig. 15 required 20 seconds of CPU time whereas computing both curves in Fig. 16 only required 1.2 CPU seconds. This demonstrates the efficiency of the DRAUSS approach relative to time integration. In the above mentioned simulations, the beam is discretized by a one-dimensional finite-difference mesh. The

difference in run time between the two methods for computing the dynamic pull-in parameters may be expected to dramatically increase when the dynamic response of 2D and 3D models of the system are simulated.
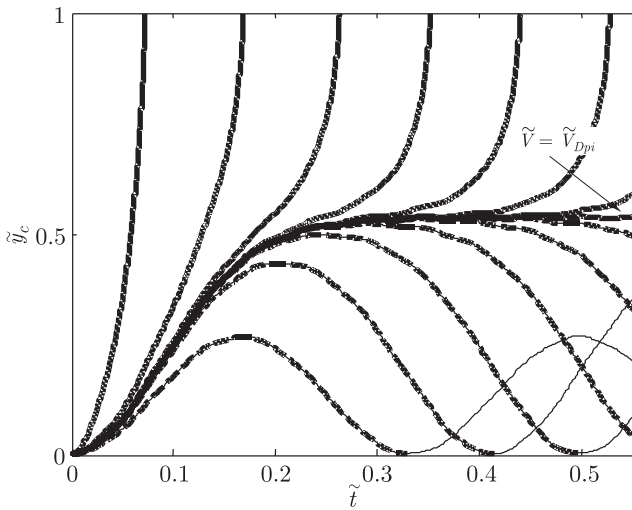

Fig. 15. Dynamic response of the voltage-driven clamped-clamped beam actuator for various values of applied voltage (for $\widetilde{g} \ll 1$, $\widetilde{E} = 1$, $\xi = 0.01$ and $\alpha = 0.3$)
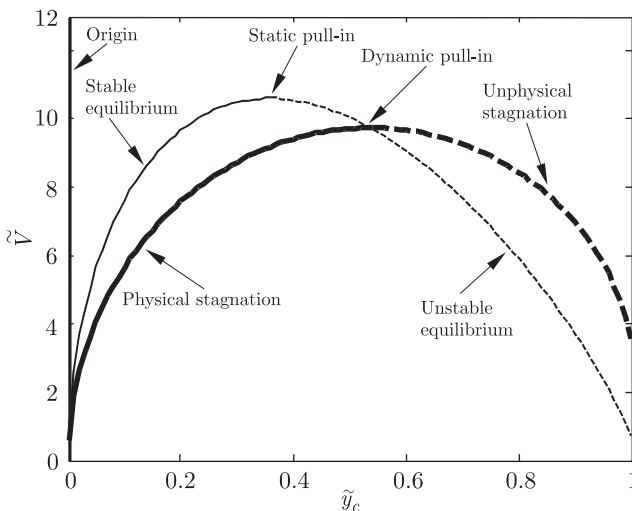

Fig. 16. Equilibrium (thin lines) and stagnation (thick lines) curves of the voltage-driven clamped-clamped beam actuator (for $\widetilde{g} \ll 1$, $\widetilde{E} = 1$, $\xi = 0.01$ and $\alpha = 0.3$)

4. Discussion

For the parallel-plates actuator the dynamic pull-in voltage is 8% lower than the static pull-in voltage. For the tilt-plate actuator, the dynamic pull-in voltage is 17% lower than the static pull-in voltage, and the dynamic pull-in charge is 26% lower than the static pull-in charge. For the clamped-clamped beam actuator, the dynamic pull-in voltage is lower by 8% relative to the static pull-in voltage.

When damping is considerable the actuators may be expected to respond quasi-statically, and higher voltages or

charges (up to the relevant static pull-in values) may be required to ensure a switching (i.e. pull-in) response.

If the pull-in instability is to be avoided for each of the actuators over the entire range of possible displacement, the parameters of the dielectric layer may be chosen such that a full travel range (i.e. $\widetilde{x} = 1$ or $\widetilde{\theta} = 1$) is achieved before pull-in occurs. For example, the voltage pull-in of the tilt-plate actuator occurs at $\widetilde{\theta}/(1 + \xi) = 0.44042$ and $\widetilde{V}^2/(1 + \xi)^3 = 0.82745$ Eq. (25). By choosing $\xi = 0.44042^{-1} - 1 = 1.2706$ a full travel range $\widetilde{\theta} = 1$ can be achieved and pull-in will not occur. This increase of 227% in the travel range will however require an increase of 342% in the actuation voltage.

5. Summary

In this work the static and the dynamic pull-in parameters of electrostatic actuators were considered, for both voltage and charge actuation. The dynamic pull-in parameters were extracted by using the DRAUSS method. This method is applicable for systems in which damping may be neglected. The method is based on static states only and it avoids the necessity of integrating the equilibrium equations in time.

The proposed method was demonstrated on two types of electrostatic actuators with a single degree-of-freedom, and on one actuator with a more realistic geometry that must be modelled as a distributed system. When the DRAUSS method is used to extract the dynamic pull-in parameters of distributed systems, the simulated dynamic pull-in voltage or charge are lower bounds of the correct parameters. This is due to the fact that some kinetic energy associated with higher mode vibrations may always remain in the system, and a total stagnation state may be energetically possible but practically very unlikely to occur [18].

REFERENCES

[1] M.J. Madou, *Fundamentals of Microfabrication: the Science of Miniaturization*, Boca Raton, Fla, CRC Press, 2002.

[2] N. Maluf, *Introduction to Microelectromechanical Systems Engineering*, Boston: Artech House, 2004.

[3] M. Tabib-Azar, *Microactuator: Electrical, Magnetic, Thermal, Optical, Mechanical, Chemical & Smart Structures*, Boston: Kluwer Academic, 1998.

[4] S.D. Senturia, *Microsystem Design*, Boston: Kluwer Academic Publishers, 2001.

[5] J.A. Pelesko and D.H. Bernstein, *Modelling MEMS and NEMS*, Boca Raton, FL: Chapman & Hall/CRC, 2003.

[6] R. Legtenberg, A.W. Groeneveld, and M. Elwenspoek, "Comb-drive actuators for large displacements", *Journal of Micromechanics and Microengineering* 6, 20–329 (1996).

[7] J.D. Grade, H. Jerman, and T.W. Kenny, "Design of large deflection electrostatic actuators", *Journal of Microelectromechanical Systems* 12, 335–343 (2003).

[8] H.J. De Los Santos, *RF MEMS Circuit Design For Wireless Communications*, Boston: Artech House, 2002.

[9] G.M. Rebeiz, *RF MEMS: Theory, Design, And Technology*, Hoboken, N.J.: Wiley-Interscience, 2003.

[10] H.A.C. Tilmans, W. De Raedt, and E. Beyne, "MEMS for wireless communications: from RF-MEMS components to RF-

MEMS-SiP", *Journal of Micromechanics and Microengineering* 13, S139–S163 (2003).

[11] S. Lucyszyn, "Review of radio frequency microelectromechanical systems technology", *IEEE Proceedings-Science Measurement and Technology* 151, 93–103 (2004).

[12] R.K. Gupta and S.D. Senturia, "Pull-in time dynamics as a measure of absolute pressure", *MEMS '97*, Nagoya, Japan, 1997.

[13] E.S. Hung and S.D. Senturia, "Generating efficient dynamical models for microelectromechanical systems from a few finite-element simulation runs", *Journal of Microelectromechanical Systems* 8, 280–289 (1999).

[14] E.K. Chan, K. Garikipati, and R.W. Dutton, "Characterization of contact electromechanics through capacitance-voltage measurements and simulations", *Journal of Microelectromechanical Systems* 8, 208–217 (1999).

[15] L.D. Gabbay, J.E. Mehner, and S.D. Senturia, "Computer-aided generation of nonlinear reduced-order dynamic macromodels I: Non-stress-stiffened case", *Journal of Microelectromechanical Systems* 9, 262–269 (2000).

[16] J.E. Mehner, L.D. Gabbay, and S.D. Senturia, "Computer-aided generation of nonlinear reduced-order dynamic macromodels II: Stress-stiffened case", *Journal of Microelectromechanical Systems* 9, 270–278 (2000).

[17] M.I. Younis, E.M. Abdel-Rahman, and A. Nayfeh, "A reduced-order model for electrically actuated microbeam-based MEMS", *Journal of Microelectromechanical Systems* 12, 672–680 (2003).

[18] D. Elata and H. Bamberger, "On the dynamic pull-in of electrostatic actuators with multiple degrees of freedom and multiple voltage sources", *Journal of Microelectromechanical Systems*, 2005, (to be published).

[19] V. Leus and D. Elata, "The dynamic response of voltage and charge driven electrostatic switches", *MEMSWAVE 2005*, Lausanne, Switzerland, 137–140 (2005).

[20] L. Castaner, J. Pons, R. Nadal-Guardia, and A. Rodriguez, "Analysis of the extended operation range of electrostatic actuators by current-pulse drive", *Sensors and Actuators A-Physical* 90, 181–190 (2001).

[21] R. Nadal-Guardia, A.M. Brosa, and A. Dehe, "Constant charge operation of capacitor sensors based on switched-current circuits", *IEEE Sensors Journal* 3, 835–842 (2003).

[22] V. Leus and D. Elata, "Fringing field effect in electrostatic actuators", *Technion – Israel Institute of Technology* ETR 2004–2, 2004.

[23] D. Elata, O. Bochobza-Degani, and Y. Nemirovsky, "Analytical approach and numerical alpha-lines method for pull-in hypersurface extraction of electrostatic actuators with multiple uncoupled voltage sources", *Journal of Microelectromechanical Systems* 12, 681–691 (2003).

[24] S. Pamidighantam, R. Puers, K. Baert, and H.A.C. Tilmans, "Pull-in voltage analysis of electrostatically actuated beam structures with fixed-fixed and fixed-free end conditions", *Journal of Micromechanics and Microengineering* 12, 458–464 (2002).

[25] O. Bochobza-Degani, D. Elata, and Y. Nemirovsky, "An efficient DIPIE algorithm for CAD of electrostatically actuated MEMS devices", *Microelectromechanical Systems* 11, 612–620 (2002).